CHEMBIOCHEM

DOI: 10.1002/cbic.200900748

# A Single-Electrode, Dual-Potential Ferrocene–PNA Biosensor for the Detection of DNA

Nina Hüsken,[a] Magdalena Gębala,[b] Wolfgang Schuhmann,[b] and Nils Metzler-Nolte*[a]

A Fc–PNA biosensor (Fc: ferrocenyl, $C_{10}H_9Fe$) was designed by using two electrochemically distinguishable recognition elements with different molecular information at a single electrode. Two Fc–PNA capture probes were therefore synthesized by N-terminal labeling different dodecamer PNA sequences with different ferrocene derivatives by click chemistry. Each of the two strands was thereby tethered with one specific ferrocene derivative. The two capture probes revealed quasi-reversible redox processes of the $Fc^{0/+}$ redox couple with a significant difference in their electrochemical half-wave potentials of $\Delta E_{1/2} = 160$ mV. A carefully designed biosensor interface, consisting of a ternary self-assembled monolayer (SAM) of the two C-terminal cysteine-tethered Fc–PNA capture probes and 6-mercaptohexanol, was electrochemically investigated by square wave (SWV) and cyclic voltammetry (CV). The biosensor properties of this interface were analyzed by studying the interaction with DNA sequences that were complementary to either of the two capture probes by SWV. Based on distinct changes in both peak current and potential, a parallel identification of these two DNA sequences was successful with one interface design. Moreover, the primary electrochemical response could be converted by a simple mathematical analysis into a clear-cut electrochemical signal about the hybridization event. The discrimination of single-nucleotide polymorphism (SNP) was proven with a chosen single-mismatch DNA sequence. Furthermore, experiments with crude bacterial RNA confirm the principal suitability of this dual-potential sensor under real-life conditions.

## Introduction

Peptide nucleic acids (PNA) are non-natural analogues, with regard to structure and properties, of DNA/RNA. In PNA, the negatively charged (deoxy)ribose phosphodiester backbone of DNA/RNA is replaced by a neutral pseudopeptide backbone of repeating *N*-(2-aminoethyl)glycine units.[1,2] Due to the non-charged backbone, PNA reveals outstanding properties such as thermodynamically and kinetically enhanced hybridization with DNA/RNA, most notably with high selectivity and excellent discrimination of single-nucleotide mismatches. Analytical and biological applications also benefit from the high chemical stability of PNA and its persistance towards nucleases and proteases.[3] These features make PNA exceptionally attractive for analytical applications such as the detection of single-nucleotide polymorphism (SNP). The use of PNA as recognition device in electrochemical DNA biosensors[4,5] has been widely investigated in the past years. Most workers pursued approaches of a label-free DNA detection, which uses the interaction between a charged free-diffusing redox mediator and the negatively charged DNA backbone for electrochemical DNA detection.[6–8] More recently, electrochemical PNA biosensors have been described, wherein the PNA capture probe carries a redox-active metal complex as a (N-terminally) covalently bound label.[9–14] Several groups have reported the synthesis of PNA derivatives with covalently linked (organo)metal complexes,[15–19] and many of these complexes carry a ferrocenyl (Fc, $C_{10}H_9Fe$) group as a redox-reversible organometallic label.[20–24] A major advantage of the use of redox-probe-conjugated PNA oligomers over free-diffusing redox mediators is the defined and permanent bonding between the redox-active species and the PNA recognition element. However, a detection mechanism that enables a facile, reliable, and distinct DNA analysis including SNP detection with a Fc–PNA biosensor has not been fully developed so far. A general issue is the "signal-off" architecture of Fc–PNA biosensors, that is, a stronger electrochemical response is observed for the flexible single strand, and only a weak response is obtained for the rigid duplex with the complementary DNA analyte. Alternative approaches that are based on the electron transfer through PNA/DNA duplexes (nanowire concept) generally face difficulties due to slow electron transfer rates.[25,26] Hence, a new detection strategy is required to fully exploit the favorable characteristics of Fc–PNA conjugates for DNA biosensing applications, which provides a facile, direct, and distinct detection of DNA target sequences.

[a] *N. Hüsken, Prof. Dr. N. Metzler-Nolte*
*Lehrstuhl für Anorganische Chemie I, Bioanorganische Chemie*
*Fakultät für Chemie und Biochemie, Ruhr-Universität Bochum*
*Universitätsstrasse 150, 44801 Bochum (Germany)*
*Fax: (+49) 234-32-14378*
*E-mail: nils.metzler-nolte@ruhr-uni-bochum.de*

[b] *M. Gębala, Prof. Dr. W. Schuhmann*
*Analytische Chemie, Elektroanalytik und Sensorik*
*Fakultät für Chemie und Biochemie, Ruhr-Universität Bochum*
*Universitätsstrasse 150, 44801 Bochum (Germany)*

*Supporting information for this article is available on the WWW under http://dx.doi.org/10.1002/cbic.200900748.*

## Results and Discussion

### Biosensor concept

With this endeavor, we designed a new Fc–PNA biosensing interface, consisting of two electrochemically distinguishable Fc–PNA conjugates **P1** and **P2** that are immobilized simultaneously on a gold electrode. Each of the two different PNA sequences serves as a specific recognition element for one particular DNA sequence, which upon hybridization selectively induces specific changes in the electrochemical response of the respective fully complementary Fc–PNA capture probe (Scheme 1). This dual-potential sensor improves the "signal-off" architecture of *Aoki*'s single-potential Fc–PNA sensor surface,[10] by providing the second Fc–PNA capture probe as an internal reference for all electrochemically detectable events.

### Probe design

The gist of this dual-potential biosensor is the association of molecular information with a certain electrochemical potential. We recently reported a straightforward method for the introduction of different ferrocene derivatives to the N terminus of PNA by click chemistry,[27,28] By means of this strategy, Fc labels with four distinguishable formal potentials ranging from $E_{1/2}=$ +250 mV to +540 mV Ag/AgCl were tethered to PNA strands. This "four-potential" labeling represents the electrochemical equivalent of the "four-color" detection in classical DNA sequencing. For the synthesis of the Fc–PNA conjugates **P1** and **P2**, two different alkyne-functionalized ferrocene derivatives were conjugated through a [2+3] Cu-catalyzed azide/alkyne cycloaddition (*click chemistry*) to different azide-functionalized PNA precursors. These PNA precursors of **P1** and **P2** were synthesized by standard Fmoc solid-phase PNA synthesis, wherein the azide function was introduced by the coupling of azido acetic acid to the free N terminus of the PNA sequence. Click reaction of the respective azido PNA precursor with ethynyl ferrocene yielded **P1** and with *N*-(3-ethylpent-1-yn-3-yl)ferrocene-carboxamide (DEPA-ferrocene) yielded **P2** (Scheme 2). The Fc–PNA conjugates were comprehensively characterized by analytical HPLC and MALDI-TOF mass spectrometry. Electro-

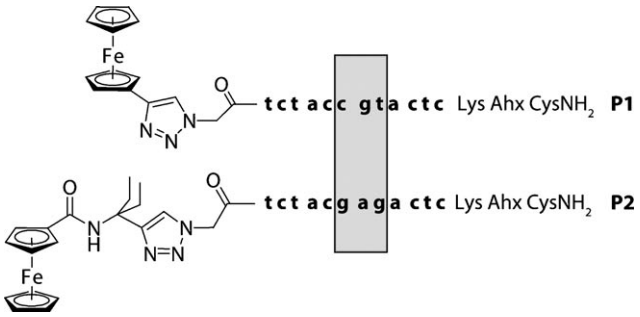


**Scheme 2.** N-terminal Fc-labeled and C-terminal thiol-modified PNA capture probes **P1** and **P2**.

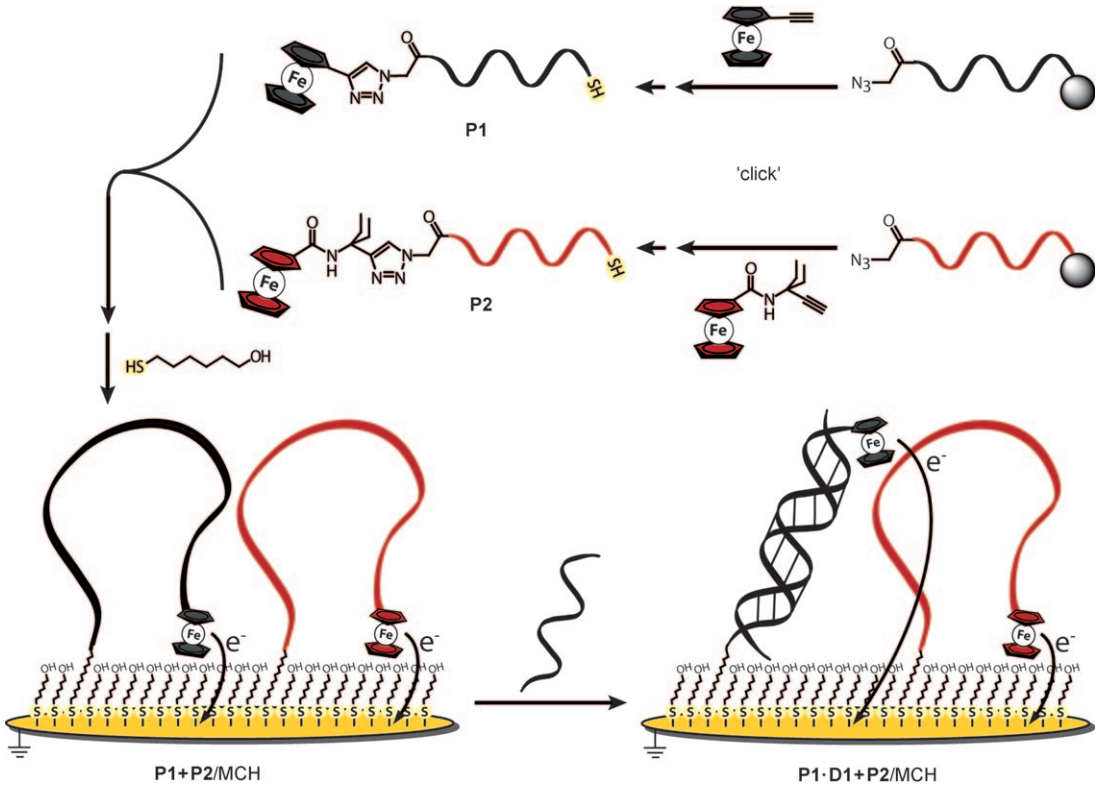


**Scheme 1.** Outline of the dual-potential Fc–PNA biosensor: Synthesis of **P1** and **P2** by click-labeling of two PNA sequences with two Fc derivatives, design of the sensor surface P1 + P2/MCH by double immobilization of capture probes P1 and P2 at one gold electrode and modification with MCH, and hybridization with DNA analyte D1.

  

chemical characterization of solutions of **P1** and **P2** with cyclic voltammetry (CV) and square wave voltammetry (SWV) revealed halfwave potentials of $E_{1/2}$ (**P1**) = 330 mV and $E_{1/2}$ (**P2**) = 490 mV vs. Ag/AgCl with a difference of $E_{1/2}$ (**P2**) - $E_{1/2}$ (**P1**) = 160 mV. The 12-mer PNA sequences of **P1** and **P2** differ by an internal triple mismatch and are C-terminally modified with a cysteine-containing peptidic linker for the immobilization on gold electrodes under formation of a Au–S linkage (Scheme 2).

### Sensor interface of binary Fc–PNA/MCH SAMs

The electrochemical biosensing properties of the Fc–PNA probes **P1** and **P2** were investigated in preliminary experiments by individual immobilization at gold microelectrodes (Ø = 100 μm), blocking of free surface positions with 6-mercaptohexan-1-ol (MCH), and subsequent hybridization with the respective complementary DNA sequence. The sensor interface **P1**/MCH reveals a SWV peak potential of $E_{1/2}$ = 330 mV vs. Ag/AgCl and **P2**/MCH of $E_{1/2}$ = 460 mV vs. Ag/AgCl, with a slightly lower difference of $E_{1/2}$ (**P2**)-$E_{1/2}$ (**P1**) = 130 mV than the respective species in solution. The conditions for the ssPNA immobilization ($c_{ssPNA}$ = 20 μM, $T$ = room temperature, $t$ = 16 h) were chosen so as to yield relatively low Fc–PNA surface concentrations of $\Gamma_{ssPNA} = 24.5 \pm 7.3$ pmol cm$^{-2}$, which correspond to ~8 ± 2% of a maximal expected surface concentration of $\Gamma_{ssPNA}$ = 300 pmol cm$^{-2}$ (reported for Cys-Tn-Fc ($n$ = 4-–6)[25,29]) and a rather large footprint of 25.3 ± 6.4 nm$^2$ per molecule. Assuming a statistical surface coverage, lateral interactions between the probe molecules can therefore be neglected.

Hybridization at the interfaces **P1**/MCH and **P2**/MCH with the respective fully complementary DNA target sequences **D1** or **D2** results at both interfaces in a significant decrease of the peak current $i_P$ (**P1**/MCH: −65%, **P2**/MCH: −55%) and a shift of the peak potentials $E_{1/2}$ to lower values (**P1**/MCH: −10 mV, **P2**/MCH: −25 mV, Figure 1). Aoki et al. observed a similar decrease in peak current for ferrocene carboxylic acid-conjugated PNA probes and proposed that this signal-off effect is due to a change in the electron transfer after formation of the PNA–DNA duplexes.[10] The flexible structure of the single-stranded PNA probe enables the ferrocene moiety to come close to the gold surface, resulting in an increased probability for the electron-transfer reaction and hence a higher current during the timescale of the SWV. The hybridization with fully complementary DNA induces structural changes by formation of the cylindrical PNA–DNA duplex, which has a higher rigidity compared to the respective PNA single strand. These structural changes affect the electrochemical response of the tethered ferrocene moiety because the constricted bending behavior of the duplex enforces a larger distance between the gold surface and the ferrocene moiety, and thereby impedes the electron transfer reaction.[30–32] A decrease of the peak current to zero was never observed upon hybridization (cf Aoki et al.[10]) and hence the remaining current (**P1**·**D1**/MCH = 35%, **P2**·**D2**/MCH = 45% of the respective ssPNA/MCH surface) can be ascribed to the residual flexibility of the PNA–DNA duplex as well as to a contribution of the peptidic $C_{10}N_3$ linker to the overall bending flexibility of the Fc-PNA(·DNA) probe. The potential shift to lower values is presumably due to the influence of the negatively charged DNA backbone on the peak potential of the $Fc^{0/+}$ redox couples because the same effect was observed in CV and SWV measurements in solutions of the respective single and double strands of **P1** and **P2** at a glassy carbon working electrode.

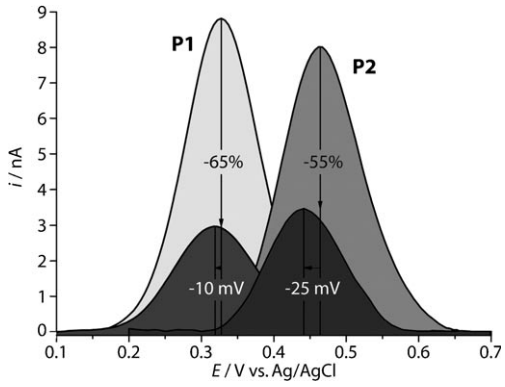


**Figure 1.** Overlay of four background-subtracted SWV (differential scans) of binary Fc–PNA interfaces consisting of Fc–PNA probes **P1** or **P2** and MCH ($f$ = 1.0 kHz, step potential = 5 mV, amplitude = 25 mV). **P1**/MCH interface before (light gray) and after (dark gray) hybridization with fully complementary DNA **D1**. **P2**/MCH interface before (light blue) and after (dark blue) hybridization with fully complementary DNA **D2**.

### Dual-potential sensor interface of ternary P1 + P2/MCH SAMs

The dual-potential biosensor interface **P1** + **P2**/MCH was constructed by coadsorption of an equimolar ratio of the capture probes **P1** and **P2** at gold electrodes and the subsequent sequential adsorption of MCH. SWV and CV measurements show two distinguishable, but overlapping redox signals for **P1** and **P2**, which reveal peak potentials of $E_{1/2}$ (**P1**) = 328 ± 2 mV and $E_{1/2}$ (**P2**) = 454 ± 4 mV vs. Ag/AgCl with a difference of 125 ± 5 mV (Figure 2). The simultaneous immobilization of **P1** and **P2** was performed under conditions equivalent to the preparation of the individual ssPNA surfaces ($c_{P1+P2}$ = 20 μM, $T$ = room temperature, $t$ = 16 h), obtaining comparable surface concentrations of $\Gamma_{P1+P2} = 21.9 \pm 2.7$ pmol cm$^{-2}$ and corresponding large footprints of 25.8 ± 3.0 nm$^2$ per moleculesurface concentrations of and corresponding large footprints of 0.08 per molecule. The resulting molar **P1**/**P2** ratio on the surface was not strictly identical to the **P1**/**P2** ratio of the buffered solution (1:1), and surface ratios ranging from **P1**/**P2** = 1:0.66 to 1:1.30 were obtained. Because no general preference for the adsorption of either **P1** or **P2** was observed, the deviation from the 1:1 ratio in solution is ascribed to kinetic instabilities during the adsorption process.

The dependence of the SWV peak currents $i_P$ on the frequency $f$ in the SWV parameters shows a strong electronic interaction between **P1** and **P2** at lower frequencies ($f$ < 0.5 kHz), presumably due to an indirect electron transfer mechanism in which **P2** reduces **P1** and therefore contributes to the peak current of **P1**. The 3D plot of SWV at various frequencies rang-

  

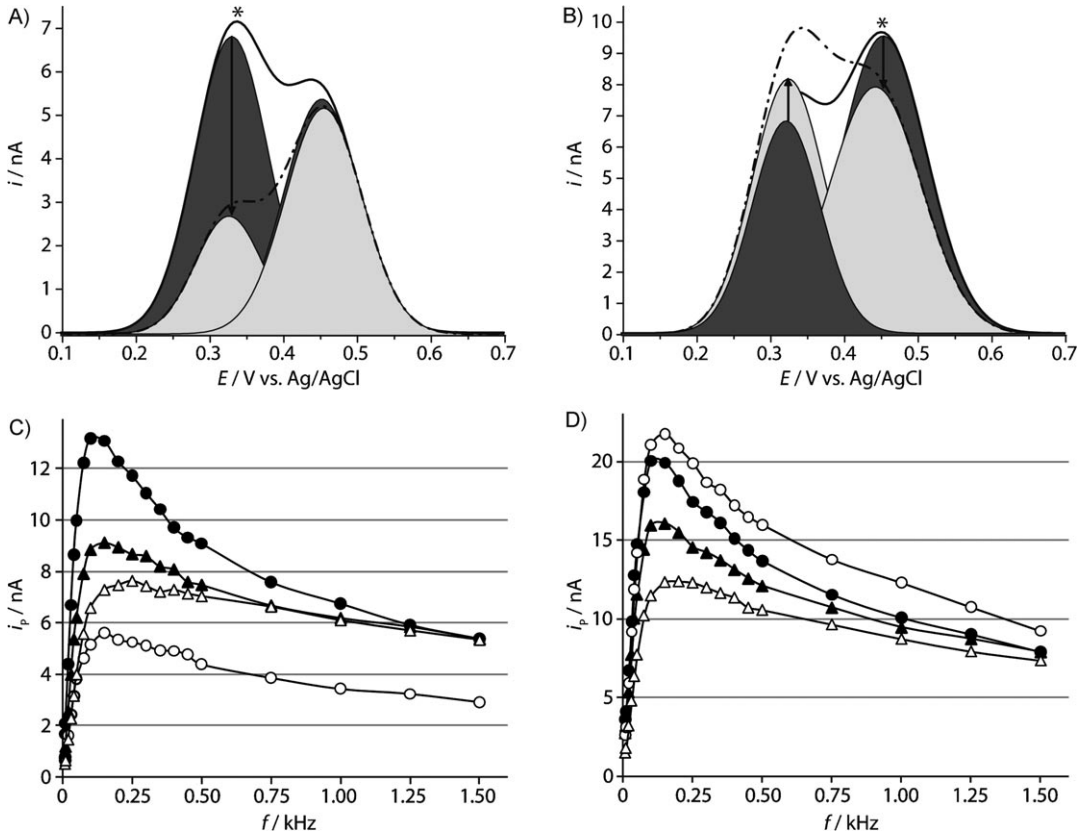


**Figure 2.** A), B) Overlay of background-subtracted SWV (differential scans; $f = 1.0$ kHz, step potential = 5 mV, amplitude = 25 mV) of the **P1** + **P2**/MCH interfaces before hybridization (——) and after hybridization with target DNA (-----). A) Hybridization with **D1** (**P1**·**D1** + **P2**/MCH interface); B) hybridization with **D2** (**P1** + **P2**·**D2**/MCH interface). Shaded curves result from the two-impulse deconvolution (see the Experimental Section) of the four demonstrated SWV: SWV deconvolution of the **P1** + **P2**/MCH interfaces before hybridization (dark gray) and after hybridization with **D1** or **D2** (light gray). The signal that results from the fully complementary Fc–PNA probe **P1** or **P2**, respectively, is marked by an asterisk. C), D) frequency $f$ dependence of the SWV peak current $i_p(f)$ corresponding to the SWV shown in graphs A) (corresponding to C)) and B) (corresponding to D)) ($i_P$ normalized to a **P1**:**P2** ratio = 1:1 at $f = 1.5$ kHz; peak currents of **P1** + **P2**/MCH interface: filled symbols. Hybridization with target DNA: empty symbols. Peak current induced by **P1** (cycles) and **P2** (triangles). Data analysis from background-subtracted, deconvolved voltammograms.

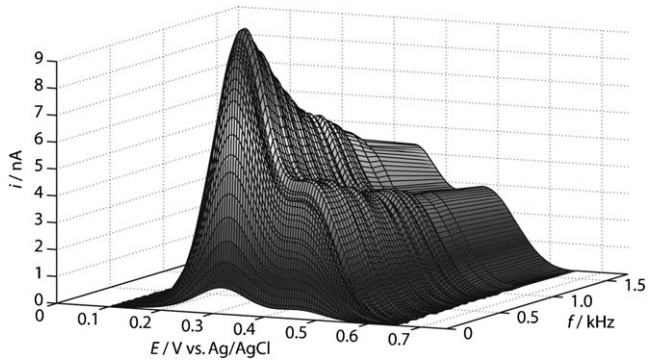


**Figure 3.** Three-dimensional plot of SWV (background subtracted differential scans, step potential = 5 mV, amplitude = 25 mV) of the **P1** + **P2**/MCH sensor surface at various frequencies ranging from $f = 8$ Hz to 1.5 kHz.

ing from $f = 8$ Hz to $f = 1.5$ kHz (Figure 3) nicely demonstrates the frequency dependence of the electronic interaction between **P1** and **P2** at the **P1** + **P2**/MCH sensor surface.

Because this secondary mechanism is kinetically largely suppressed at higher frequencies ($f > 0.5$ kHz), voltammograms at $f = 1.0$ kHz were used for the following biosensor studies. SWV overlays **A** and **B** in Figure 2 show the influence of hybridization with target DNA sequences **D1** and **D2** on the SWV signal of the **P1** + **P2**/MCH surface. UV melting experiments proved that **D1** is fully complementary to capture probe **P1** ($T_m$ = 54.9 °C), whereas no hybridization was observed with **P2**. The reverse is true for **D2** (**P2**·**D2**: $T_m$ = 60.0 °C, **P1**/**D2**: no hybridization, see the Supporting Information). Graph **A** shows that the hybridization with **D1** at the **P1** + **P2**/MCH interface results in a marked decrease in the peak current of **P1**, whereas the signal of **P2** remains nearly unaffected. The potential shift that was observed at the **P1**/MCH-modified electrode reflects that at the **P1** + **P2**/MCH-modified surface with an increase of the potential difference $\Delta\Delta E_P = +8.3$ mV (Figure 4). Hybridization with **D2** (graph B)) shows an analogous decrease of the potential difference of −11.5 mV and the expected decrease of the **P2** peak current. Interestingly, a simultaneous increase of the **P1** signal is observed, which can be explained by an enhancement of the secondary electron transfer mechanism due to the decrease of the potential difference between **P1** and **P2**. Thus, with the **P1** + **P2**/MCH biosensor interface a clear distinction between fully and non-complementary DNA based on changes

  

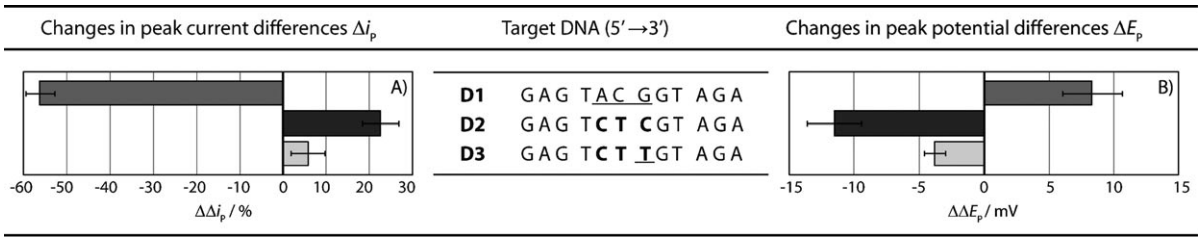


**Figure 4.** Incubation of the **P1**+**P2**/MCH gold surfaces with target DNA sequences **D1**, **D2** and **D3** (bold letters: mismatch to **P1**, underlined letters: mismatch to **P2**). A) Percent change of the peak currents $\Delta i_P$ (**P1**) and $\Delta i_P$ (**P2**) upon hybridization with target DNA. $\Delta\Delta i_P = \Delta i_P$ (**P1**)$-\Delta i_P$ (**P2**). B) $\Delta\Delta E_P$: Change of the peak separation $\Delta E_P = E_P$ (**P2**)$-E_P$ (**P1**) upon hybridization with target DNA (**D1**: medium gray, **D2**: dark gray, **D3**: light gray). Raw data were determined from background subtracted and deconvolved SWV. SWV parameters: $f = 1.0$ kHz, amplitude = 25 mV, step potential = 5 mV. Error bars were determined from three measurements.

in potential difference and peak current is possible with single SWV measurements (Figure 4).

The electrochemical response upon the hybridization with target DNA can be visualized and analyzed easily by subtracting the SWV data of the sensor surface **P1**+**P2**/MCH (Figure 5) from the SWV data of the sensor surfaces **P1**·**D1**+**P2**/MCH or **P1**+**P2**·**D2**/MCH, respectively, obtained after hybridization with **D1**, or **D2**. By this mathematical operation, a hybridization-induced current decrease results in a negative signal, whereas non-affected signals of the respective noncomplementary internal reference decrease to zero. This data presentation simplifies a complex data analysis consisting of background subtraction and signal deconvolution, to readily provide a clear-cut electrochemical response about the hybridization event.

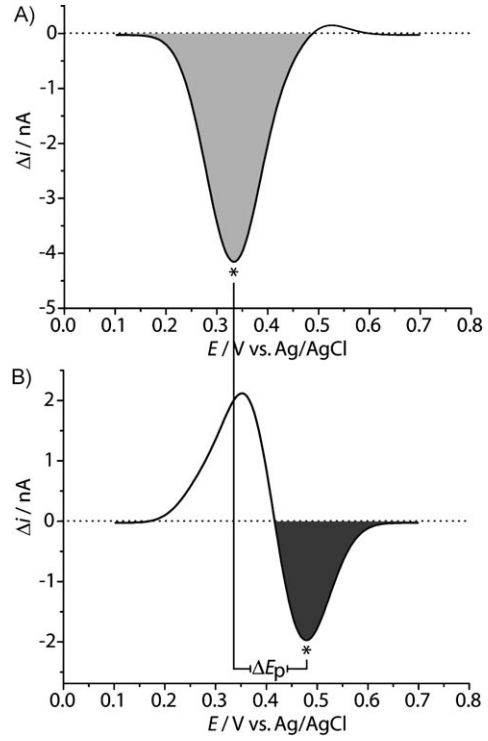


**Figure 5.** Subtraction of SWV data (differential scans; $f = 1.0$ kHz, step potential = 5 mV, amplitude = 25 mV) of the sensor surface **P1**+**P2**/MCH from the surfaces obtained after hybridization with target DNA A) **D1** ($\Delta i = i$(**P1**·**D1**+**P2**/MCH)$-i$(**P1**+**P2**/MCH)) and B) **D2** ($\Delta i = i$(**P1**+**P2**·**D2**/MCH)$-i$(**P1**+**P2**/MCH)).

Detection of single-nucleotide polymorphism (SNP) was examined by incubation of the **P1**+**P2**/MCH sensor interface with target DNA **D3**, which exhibits a thermodynamically stable internal mismatch with **P2** (**P2**·**D3**: $T_m = 47.7\,^{\circ}$C) and is noncomplementary to **P1**. Figure 4 shows, that **D3** induces changes in peak current and potential difference with the same tendency as **D2**, but reveals both effects to a significantly less extent than its fully complementary analogue **D2**. This demonstrates that the **P1**+**P2**/MCH sensor surface can readily detect DNA target sequences, which are fully complementary to PNA probes **P1** or **P2**. At the same time, the sensor system discriminates fully complementary sequences from mismatch sequences by their electrochemical signature, even when they do hybridize to one of the PNA sequences at room temperature. Hence, in this setup there is no need for a thermal annealing step.

## Conclusions

In conclusion, the presented dual-potential Fc–PNA biosensor is a promising and reliable tool for the analysis of DNA target sequences. This biosensor is qualified to identify two different DNA target sequences with one biosensor surface in a single SWV measurement, due to selective and clear changes in peak current and potential. At the same time it provides a ready discrimination of SNP sequences. It reveals distinct and easy-to-interpret electrochemical signals due to the second capture probe, which serves as an internal reference for all detectable electrochemical parameters. A simple mathematical analysis of the primary electrochemical response then yields a clear-cut electrochemical signal of the hybridization event. Moreover, the dual-potential design measures simultaneously the interaction of a DNA analyte sequence with two different, electrochemically localized PNA probes on one and the same electrode surface. Thereby, one single experiment provides two different sets of sequence information on the DNA analyte, which are derived from two independent PNA–DNA interactions. Given the dual-potential design, the data for both strains are obtained under constant conditions of a single experiment, which ensures maximal data integrity and comparability. Evidently, this biosensor concept is expandable to a single-elec-

  

trode sensor with a multipotential/multiple capture probes recognition interface. Furthermore, the favorable properties of PNA in terms of hybridization characteristics, chemical stability and its high stability towards nucleases and proteases facilitate a direct analysis of biological samples with the herein-presented PNA biosensor. In an exploratory experiment, the dual potential **P1**+**P2**/MCH sensor surface was incubated with crude bacterial RNA extracts from *P. putida* and *E. coli*. CV and SWV were of good quality and showed that the sensor surface was fully stable towards the treatment with the crude cell lysates. Moreover, no interfering signals due to additional cell ingredients or salts were detected. The expected trends in peak current and potential changes were observed for both bacterial stems, however the response to the purified, high-quality 12-mer DNA oligomers **D1** and **D2**, as shown in Figure 4, was clearly developed to a greater extent. Nonetheless, this experiment demonstrates that this concept is suitable for real-life applications in principle. Obviously, for this purpose the actual surface design still needs to be optimized towards improved analytical properties. Such optimization towards a practical application is currently under way in our laboratory.

## Experimental Section

**Reagents:** All reagents and HPLC-grade solvents were purchased from Acros (Geel, Belgium), Aldrich/Sigma/Fluka (Deisenhofen, Germany), E. Merck (Darmstadt, Germany), J. T. Baker (Deventer, The Netherlands), Novabiochem (Laufelfingen, Switzerland) and IRIS Biotech (Marktredwitz, Germany) and were used without further purification. All aqueous solutions were prepared with Millipore $H_2O$ and filtered with a 0.22 μm sterile syringe filter before use. PNA oligomers were synthesized from Fmoc/Bhoc-protected PNA monomers, which were purchased from Link Technologies (Edinburgh, Scotland) and ASM (Hannover, Germany). The preloaded polystyrene resin TentaGel R PHB Cys(Trt)Fmoc was purchased from Rapp Polymers (Tübingen, Germany). L-Amino acids were purchased from Novabiochem (Laufelfingen, Switzerland). HPLC-purified DNA oligonucleotides were purchased from MWG Biotech (Ebersberg, Deutschland). All solutions were freshly prepared before use. HPLC fractions of all products were frozen in liquid $N_2$ and lyophilized by using an Edwards Modulyo freeze dryer.

**Instrumentation and methods:** MALDI-TOF mass spectra were measured on a Bruker Daltonics Autoflex in linear mode with positive polarity by using sinapic acid as the matrix. HPLC analysis and purification was performed on a customized Varian ProStar 210 System, equipped with a PDA detector and autosampler by using Varian DynaStar C-18 reversed-phase columns for analytical (250× 4 mm) and preparative (250×21 mm) runs. Analytical (flow rate: 1.0 mL $min^{-1}$) and preparative (flow rate: 4.7 mL $min^{-1}$) runs were performed with a linear gradient of A (Millipore $H_2O$ containing 0.1% *v/v* TFA) and B (MeCN (Baker HPLC-grade), containing 0.1% *v/v* TFA). Analytical runs: $t=0$ min 5% B, $t=20$ min 80% B, $t=25$ min 5% B. Preparative runs: $t=0$ min 5% B, $t=12$ min 15% B, $t=32$ min 40% B, $t=50$ min 80% B, $t=60$ min 5% B. All samples were filtrated before injection by using a 0.22 μm syringe filter. Spectra were recorded at 254 nm and 25 °C, retention times ($t_R$ [min]) were noted in each case. UV melting experiments were performed with the UV/vis spectrophotometer Varian Cary 100 Conc equipped with a 6×6 multicell block and Peltier thermostat.

**Solid-phase synthesis:** SPPS was performed manually in 5 mL polypropylene one-way syringes as reaction vessels, which were equipped with a frit at the bottom. They were filled with polystyrene resin beads (50 mg, 9 μmol) of TentaGel R PHB Cys(Trt)Fmoc (loading: 0.18 mmol $g^{-1}$). The resin was swollen in DMF before use for 1 h. All reactions were performed on a mechanical shaker with 400 rpm, withdrawing/suctioning the freshly prepared solutions (~3–4 mL) into and out of the syringe. Fmoc/Bhoc-protected PNA monomers (5 equiv) were preactivated in Eppendorf tubes before every coupling step for 2 min with HATU (4.5 equiv) in DMF, by adding $iPr_2EtN$ and 2,6-lutidine (10 equiv each) (A(bhoc)-PNA-monomer: 5 min, C(bhoc)-PNA-monomer: 7 min). The L-amino acids Fmoc-Ahx and Fmoc-Lys(Boc)-OH were preactivated in an analogous manner with TBTU and $HOBt·H_2O$ (4.5 equiv each). For each coupling step, the resin beads were treated with the activated acid under vibration (50 °C, 20 min) and subsequently washed with DMF. The coupling step was monitored with the Kaiser test. Double Fmoc deprotection was performed with piperidine (20%, *v/v*) in DMF (2 min+10 min). The resin beads were then washed successively with DMF, $CH_2Cl_2$ and DMF. The whole procedure (deprotection, coupling, monitoring) was repeated for every PNA monomer until the PNA sequence was completed. The resin was washed and shrunk with MeOH (30 min) and dried under vacuum. Final cleavage of the PNA oligomer from the resin and the deprotection of all Bhoc, Trt, and Boc side-chain-protecting groups were simultaneously performed in TFA/TIS/phenol (85:5:10, *v/v/v*; 2 h + 1 h). Following the removal of TFA under reduced pressure, the crude product was precipitated with ice-cold $Et_2O$, washed twice with ice-cold $Et_2O$, and each time centrifuged (10 min, 8000 rpm). The obtained crude oligomer was lyophilized in $MeCN/H_2O$, purified and analyzed with RP-HPLC, and finally characterized with ESI or MALDI-TOF mass spectrometry.

**Synthesis of azidoacetic acid functionalized precursors of P1 and P2.** N-terminal azide functionalization of the PNA oligomers of **P1** and **P2** was performed on polystyrene resins that were preloaded with the respective PNA sequence, and synthesized according to the general SPPS procedure. The solid-phase coupling of 2-azidoacetic acid followed the Fmoc deprotection of the last PNA monomer of the respective PNA sequence. 2-Azidoacetic acid (5 equiv) was preactivated for 3 min in an Eppendorf tube with TBTU and $HOBt·H_2O$ (4.5 equiv each) in DMF, with $iPr_2EtN$ and 2,6-lutidine (10 equiv each). The polystyrene resin (50 mg, 9 μmol), which was preloaded with the respective PNA sequence (PNA precursor of **P1**: H-t c t a c c g t a c t c Lys Ahx $CysNH_2$, precursor of **P2**: H-t c t a c g a g a c t c Lys Ahx $CysNH_2$), was treated with the activated acid under vibration at RT for 1 h. The resin was then successively washed with DMF, $CH_2Cl_2$, and DMF, washed and shrunk with MeOH (30 min) and dried under reduced pressure. After splitting of the resin beads in a ratio of 1:9, the cleavage according to the general procedure was performed at 5 mg (0.9 μmol) of the azido–PNA-loaded resins to yield the free azide-functionalized PNA precursors of **P1** and **P2** for characterization. Azide-functionalized precursor of **P1** ($M=3607.6$ g $mol^{-1}$): Yield: 80% (2.6 mg, 0.72 μmol). MALDI-TOF MS: *m/z* (%): 3609.6 $[M+H]^+$ (100).[28] Azide-functionalized precursor of **P2** ($M=3656.6$ g $mol^{-1}$): Yield 82% (2.7 mg, 0.74 μmol). MALDI-TOF MS: *m/z* (%): 3659.7 $[M+H]^+$ (100).

**Synthesis of Fc–PNA conjugates P1 and P2:** Conjugation of ferrocene by [2+3]-azide–alkyne cycloaddition was performed under inert conditions on the remaining polystyrene resins (45 mg 8.1 μmol), which were preloaded with the azide-functionalized PNA precursors of **P1** and **P2**. All solvents were taken out of crown cap

  

bottles, and Eppendorf tubes were flushed with $N_2$ before use. Following the synthesis of the azide–alkyne-functionalized PNA oligomers, the syringe containing the shrunk resin beads was flushed with $N_2$, and the resin was washed and swollen for 1 h with dry DMF. The following solutions were prepared: $iPr_2EtN$ and 2,6-lutidine (each 10 equiv) in DMF, the respective alkyne-functionalized ferrocene derivative (1%, 5 equiv) in DMF and CuBr (1%, 1 equiv) in MeCN. These solutions were successively introduced into the syringe containing the preloaded resin. This reaction mixture was vibrated for the given reaction time at ambient temperature. Subsequently, the resin was successively washed with DMF, $CH_2Cl_2$, MeCN, $CH_2Cl_2$, and DMF. After washing and shrinking of the resin in MeOH (30 min) and drying under reduced pressure, **P1** and **P2** were cleaved from the resin by following the general procedure and obtained as white solids.

*Synthesis of **P1***: The resin (45 mg, 8.1 μmol), which was preloaded with the azide-functionalized PNA precursor $N_3$-$CH_2$CO-t c t a c c g t a c t c Lys Ahx Cys$NH_2$ was converted according to the general procedure with ethynylferrocene (8.51 mg, 40.5 μmol, 5 equiv) in 2 d. Cleavage from the resin by following the general procedure yielded **P1** as a yellowish solid. **P1** (3817.6 g mol$^{-1}$): Yield: 76% (23.6 mg, 6.2 μmol). HPLC: $t_R = 13.7$ min, 100%. MALDI-TOF MS: *m/z* (%): 3819.8 $[M+H]^+$ (100).[28]

*Synthesis of **P2***: The resin (45 mg, 8.1 μmol), which was preloaded with the azide-functionalized PNA precursor $N_3$-$CH_2$CO-t c t a c g a g a c t c Lys Ahx Cys$NH_2$ was converted according to the general procedure with DEPA-ferrocene (13.12 mg, 40.5 μmol, 5 equiv) in 2 d. Cleavage from the resin by following the general procedure yielded **P2** as a yellowish solid. **P2** (3979.82 g mol$^{-1}$): Yield: 73% (23.5 mg, 5.9 μmol). HPLC: $t_R = 13.5$ min, 100%. MALDI-TOF MS: *m/z* (%): 3986.9 $[M+H]^+$ (100).

**Electrochemical measurements:** Square wave voltammetry (SWV) and cyclic voltammetry (CV) measurements were recorded by using a microAutolab III/FRA2 potentiostat (Eco Chemie B.V., Utrecht, The Netherlands) operated by using the GPES 4.7 software. The measurements were performed with a three-electrode electrochemical cell placed in a Faraday cage. A platinum wire was used as the counter electrode, Ag/AgCl (in 3 M KCl) was used as reference electrode and the bare/modified gold-microelectrodes (diameter: 100 μm) served as working electrodes. As electrolyte solution, a phosphate buffer solution (2.5 mM, pH 7.0) containing $NaClO_4$ (0.1 M) was used, which was purged with argon gas for 15 min for removal of dissolved gases. SWV was performed by scanning from 0.0–0.7 V at an amplitude of 25 mV and a step potential of 5 mV. Various frequencies were applied, as specified underneath the respective graph/table. Raw square wave data were obtained as ASCII files and analyzed with OriginPro 8G (OriginLab, Northampton, MA, USA). Square wave voltammograms were first background subtracted and subsequently subjected to a deconvolution by applying a regular Gauss function and assuming two impulses (quality of the Gauss fit: cor. $R^2 > 0.99958$, $\chi^2 < 5.58 \times 10^{-21}$). Raw data for peak current $i_P$ and peak potential $E_P$ were collected from the deconvolved voltammograms. Peak current data $i_P$ of Figure 2 and were obtained after adjusting the peak currents $i_P$ of **P1** and **P2** to a ratio of **P1**/**P2** = 1:1 (at $f = 1.5$ kHz), to assure an accurate comparability.

**Electrode fabrication and preparation:** All electrochemical experiments at modified gold-surfaces were performed with homemade polycrystalline gold microelectrodes (diameter: 100 μm). After preparation by sealing a 100 μm gold wire (Goodfellow, Bad Nauheim, Germany) into a soda glass capillary (Ø = 1 mm; Hilgenberg GMBH, Malsfeld, Germany), the gold surfaces were exposed by polishing with sand paper. Then the gold surfaces were first mechanically polished with wet alumina slurries (particle sizes: 0.3 μm, 0.05 μm; Leco, St. Joseph, USA) on polishing cloth (Heraeus, Weinheim, Germany), afterwards they were rinsed with Millipore $H_2O$, polished on a wet polishing cloth to remove remaining adsorbed alumina traces, and finally electrochemically polished by performing cyclic voltammetry in $H_2SO_4$ (0.5 M) between 0.0–1.7 V vs. Ag/AgCl (in 3 M KCl) at a scan rate of $v = 0.1$ V s$^{-1}$ until stable oxidation/reduction currents of the formed gold oxide proved that the gold surface was clean (about 50 cycles). Subsequently, the microscopic surface area $A_{real}$ of the gold electrode was determined from cyclic voltammetry between 0–1.4 V in phosphate buffer (0.1 M, pH 7.4; scan rate $v = 0.1$ V s$^{-1}$) according to the equation $A_{real} = Q_{AuO,exp}/(\sigma_{AuO,th} \times v)$, with $\sigma_{AuO,th}$: theoretically calculated charge density for the reduction of one monolayer of chemisorbed oxygen, $\sigma_{AuO,th} = 482$ μC cm$^{-2}$;[33] $Q_{AuO,exp}$: experimentally determined charge required for the reduction of gold oxide formed through CV.[34] Surface roughness factors $R = A_{real}/A_{geometric}$ ($A_{geometric} = 7.85 \times 10^{-3}$ mm$^2$ for Ø = 0.1 mm) of $R = 1.5$ to 2.0 were obtained. After rinsing with Millipore $H_2O$, the freshly prepared gold electrodes were used right away for the immobilization process to avoid contamination of the gold surface.

**Immobilization of P1, P2, and MCH:** All surface modifications were performed by dip-coating the freshly prepared gold microelectrodes in solutions (20 μL) of the respective Fc–PNA conjugate(s), DNA oligomer or 6-mercaptohexan-1-ol (MCH). Dip-coating was carried out in 0.2 mL Eppendorf tubes, which were placed for all modification processes into a humid chamber to avoid evaporation. Subsequent to every incubation step, the electrodes were thoroughly rinsed with Millipore $H_2O$ for 20 s to remove excess of reagent and loosely bound material. The ssPNA surface concentration $\Gamma_{ssPNA}$ was determined from cyclic voltammetry (0–0.7 V; $v = 0.1$ V s$^{-1}$) in phosphate buffer solution (2.5 mM, pH 7.0) containing $NaClO_4$ (0.1 M) from the charge $Q$ required for the complete oxidation of the PNA-tethered ferrocene moieties by applying the equation $\Gamma = Q/nFA_{real}$ ($n$: number of electrons; $F$: Faraday constant; $A_{real}$: microscopic surface area of the bare gold electrode).[35] The footprint per molecule corresponds to $1/(\Gamma \cdot N_A)$ ($N_A$: Avogadro's number).

**Preparation of binary Fc–PNA/MCH SAMs:** For immobilization of a single Fc–PNA conjugate **P1** or **P2**, the freshly prepared gold-microelectrode was incubated with a solution of the respective Fc–PNA conjugate (20 μM) in a 1:1 mixture of phosphate buffer (0.1 M, pH 7.4) and MeCN overnight at ambient temperature. Subsequently, the Fc–PNA-modified gold-electrodes were sequentially modified by incubating the electrodes with a solution of MCH (1 mM) in phosphate buffer (0.1 M, pH 7.4) for 4 h at ambient temperature, to block all remaining free surface positions, to remove unspecifically adsorbed Fc–PNA conjugates, and to avoid unspecific adsorption of DNA.

**Preparation of ternary P1 + P2/MCH SAMs:** For double-immobilization, the Fc–PNA conjugates **P1** and **P2** were co-adsorbed by incubating a gold-microelectrode with a solution of **P1** and **P2** (20 μM, molar ratio 1:1) in a 1:1 mixture of phosphate buffer (0.1 M, pH 7.4) and MeCN for overnight at ambient temperature. The subsequent sequential modification with MCH was carried out as described above.

**Hybridization with DNA oligomers:** For hybridization of immobilized single-stranded Fc–PNA conjugates with different DNA oligomers, the **P1**/MCH, **P2**/MCH or **P1** + **P2**/MCH-modified gold electro-

  

des were incubated with solutions of the respective DNA oligomer (50 μM) in phosphate buffer (0.1 M, pH 7.4) for 4 h at ambient temperature.

**Abbreviations:** PNA oligomers are written from the N to the C terminus, DNA oligomers from the 5′ to the 3′ terminus. Nucleobases are denoted by their common abbreviations in DNA; small letters indicate PNA monomers. Ahx: aminohexanoic acid; Bhoc: benzhydryloxycarbonyl; Boc: *tert*-butyloxycarbonyl; cor. $R^2$: corrected coefficient of determination; DEPA: diethylpropargylamine; DMF: *N*,*N*-dimethyl formamide; Fc: ferrocenyl ($CpFeC_5H_4$); FcH: ferrocene ($Cp_2Fe$); Fmoc: fluorenylmethoxycarbonyl; HATU: 2-(1*H*-7-azabenzotriazol-1-yl)–1,1,3,3-tetramethyl uronium hexafluorophosphate; HOBt: 1-hydroxy-1*H*-benzotriazole; MCH: 6-mercaptohexan-1-ol; $R^2$ SPPS: solid-phase peptide/PNA synthesis; TBTU: *O*-(Benzotriazol-1-yl)-*N*,*N*,*N*′,*N*′-tetramethyluronium tetrafluoroborate; TFA: trifluoroacetic acid; TIS: triisopropyl silane; Trt: trityl.

## Acknowledgements

*The authors thank the European Commission in the framework of the project INTCHEM (MEST-CT-2005-020681) and the Ruhr-Universität Research School for financial support. The Research Department Interfacial Systems Chemistry (RD-IFSC) at the Ruhr-Universität is also gratefully acknowledged for support of this work. N.H. and N.M.-N. are grateful to Prof. F. Narberhaus and Dr. B. Klinkert (Ruhr-Universität Bochum) for helpful discussions.*

**Keywords:** biosensors · DNA detection · electroactive monolayers · ferrocene · peptide nucleic acids

[1] P. E. Nielsen, M. Egholm, R. H. Berg, O. Buchardt, *Science* **1991**, *254*, 1497 – 1500.
[2] E. Uhlmann, A. Peyman, G. Breipohl, D. W. Will, *Angew. Chem.* **1998**, *110*, 2954 – 2983; *Angew. Chem. Int. Ed.* **1998**, *37*, 2796 – 2823.
[3] T. Ratilainen, A. Holmén, E. Tuite, P. E. Nielsen, B. Nordén, *Biochemistry* **2000**, *39*, 7781 – 7791.
[4] J. Wang, *Biosens. Bioelectron.* **1998**, *13*, 757 – 762.
[5] J. Wang, E. Palecek, P. E. Nielsen, G. Rivas, X. Cai, H. Shiraishi, N. Dontha, D. Luo, P. A. M. Farias, *J. Am. Chem. Soc.* **1996**, *118*, 7667 – 7670.
[6] M. Steichen, Y. Decrem, E. Godfroid, C. Buess-Herman, *Biosens. Bioelectron.* **2007**, *22*, 2237 – 2243.
[7] T. H. Degefa, J. Kwak, *J. Electroanal. Chem.* **2008**, *612*, 37 – 41.
[8] M. Gebala, L. Stoica, S. Neugebauer, W. Schuhmann, *Electroanalysis* **2009**, *21*, 325 – 331.
[9] X. Luo, M.-H. Lee Thomas, I. M. Hsing, *Anal. Chem.* **2008**, *80*, 7341 – 7346.
[10] H. Aoki, H. Tao, *Analyst* **2007**, *132*, 784 – 791.
[11] N. Metzler-Nolte in *Bioorganometallics* (Ed. G. Jaouen), Wiley-VCH, Weinheim, **2006**, pp. 125 – 179.
[12] A. Maurer, H.-B. Kraatz, N. Metzler-Nolte, *Eur. J. Inorg. Chem.* **2005**, 3207 – 3210.
[13] C. Fan, K. W. Plaxco, A. J. Heeger, *Proc. Natl. Acad. Sci. USA* **2003**, *100*, 9134 – 9137.
[14] R. Y. Lai, D. S. Seferos, A. J. Heeger, G. C. Bazan, K. W. Plaxco, *Langmuir* **2006**, *22*, 10796 – 10800.
[15] C. Baldoli, S. Maiorana, E. Licandro, G. Zinzalla, D. Perdicchia, *Org. Lett.* **2002**, *4*, 4341 – 4344.
[16] S. Maiorana, E. Licandro, D. Perdicchia, C. Baldoli, B. Vandoni, C. Giannini, M. Salmain, *J. Mol. Catal. B* **2003**, *204*, 165 – 175.
[17] A. A. Mokhir, R. Stiebing, R. Krämer, *Bioorg. Med. Chem. Lett.* **2003**, *13*, 1399 – 1401.
[18] R. Hamzavi, T. Happ, K. Weitershaus, N. Metzler-Nolte, *J. Organomet. Chem.* **2004**, *689*, 4745 – 4750.
[19] S. I. Kirin, I. Ott, R. Gust, W. Mier, T. Weyhermueller, N. Metzler-Nolte, *Angew. Chem.* **2008**, *120*, 969 – 973; *Angew. Chem. Int. Ed.* **2008**, *47*, 955 – 959.
[20] A. Hess, N. Metzler-Nolte, *Chem. Commun.* **1999**, 885 – 886.
[21] J. C. Verheijen, G. A. van der Marel, J. H. van Boom, N. Metzler-Nolte, *Bioconjugate Chem.* **2000**, *11*, 741 – 743.
[22] C. Baldoli, L. Falciola, E. Licandro, S. Maiorana, P. Mussini, P. Ramani, C. Rigamonti, G. Zinzalla, *J. Organomet. Chem.* **2004**, *689*, 4791 – 4802.
[23] A. M. Sosniak, G. Gasser, N. Metzler-Nolte, *Org. Biomol. Chem.* **2009**, *7*, 4992 – 5000.
[24] R. Ikeda, S. Kitagawa, J. Chiba, M. Inouye, *Chem. Eur. J.* **2009**, *15*, 7048 – 7051.
[25] A. Paul, R. M. Watson, P. Lund, Y. Xing, K. Burke, Y. He, E. Borguet, C. Achim, D. H. Waldeck, *J. Phys. Chem. C* **2008**, *112*, 7233 – 7240.
[26] A. Paul, S. Bezer, R. Venkatramani, L. Kocsis, E. Wierzbinski, A. Balaeff, S. Keinan, D. N. Beratan, C. Achim, D. H. Waldeck, *J. Am. Chem. Soc.* **2009**, *131*, 6498 – 6507.
[27] G. Gasser, N. Hüsken, S. D. Köster, N. Metzler-Nolte, *Chem. Commun.* **2008**, 3675 – 3677.
[28] N. Hüsken, G. Gasser, S. D. Köster, N. Metzler-Nolte, *Bioconjugate Chem.* **2009**, *20*, 1578 – 1586.
[29] R. C. Mucic, M. K. Herrlein, C. A. Mirkin, R. L. Letsinger, *Chem. Commun.* **1996**, 555 – 557.
[30] A. Anne, A. Bouchardon, J. Moiroux, *J. Am. Chem. Soc.* **2003**, *125*, 1112 – 1113.
[31] A. Anne, C. Demaille, *J. Am. Chem. Soc.* **2006**, *128*, 542 – 557.
[32] A. Anne, C. Demaille, *J. Am. Chem. Soc.* **2008**, *130*, 9812 – 9823.
[33] U. Oesch, J. Janata, *Electrochim. Acta* **1983**, *28*, 1237 – 1246.
[34] J. C. Hoogvliet, M. Dijksma, B. Kamp, W. P. Van Bennekom, *Anal. Chem.* **2000**, *72*, 2016 – 2021.
[35] A. J. Bard, L. R. Faulkner in *Electrochemical Methods. Fundamentals and Applications*, 2nd ed., Wiley, New York, **2001**.

Received: December 7, 2009
Revised: April 25, 2010
Published online on July 2, 2010

  